Influence of Porosity on Plane Strain Tensile Crack-Tip Stress Fields in Elastic-Plastic Materials: Part II

Y. Miao
Graduate Research Assistant.

W. J. Drugan
Professor,
Mem. ASME.

Department of Engineering Mechanics and
Astronautics,
1415 Johnson Drive,
University of Wisconsin-Madison,
Madison, WI 53706

This paper continues the investigation of Drugan and Miao (1992). There we studied analytically the influence of a uniform porosity distribution on the stress field near a plane strain tensile crack tip in ductile (elastic-ideally plastic) material, assuming that material very near the tip is at yield at all angles about the tip. Our solutions exhibited completely continuous stress fields for porosity f ≤ 0.02979, but for higher porosities they involved radial surfaces of radial normal stress jumps. Here we investigate whether, for this higher range of porosity, relaxing our assumption of yield at all angles about the tip will facilitate solutions exhibiting fully continuous stress fields. The answer to this is shown to be yes, with a single near-tip sector assembly providing such solutions for this entire higher porosity range. On either side of the crack symmetry plane, this solution configuration consists of a leading plastic sector possessing radial stress characteristics ("generalized centered fan"), followed by a plastic sector of constant Cartesian components of stress, followed finally by a sector of purely elastic material adjacent to the crack flank. The angular extents of these sectors vary substantially with porosity level. In regions of purely elastic response, we have accounted for the influence of porosity on the overall, or effective, elastic moduli. Among the interesting features of these new solutions are a significantly enlarged generalized centered fan sector as compared to that of the fully plastic Part I solutions for the same f values, and for f values just slightly above the 0.02979 level, a narrow elastic sector exists in which stresses vary so rapidly with angle that they appear to be nearly discontinuous. This rapid variation spreads out as the elastic sector enlarges with increasing f, and, in contrast to the fully plastic solutions, the radial normal component of stress becomes negative near the crack flank.

1 Introduction

This paper continues the investigation begun in Drugan and Miao (1992), hereafter referred to as Part I. That study provided an analytical first examination of the influence of the entire range of material porosity level on the stress field near a stationary plane strain tensile crack tip in ductile (elastic-ideally plastic) material with a uniform porosity distribution, which arises approximately in, e.g., incompletely sintered or previously deformed metals and alloys. Such porosity also occurs in hot-isostatic-pressed material that is subjected to a

subsequent heat treatment, since gas trapped at high pressures then opens voids. We assumed that the material is at yield at all angles around the crack tip, obeying the Gurson-Tvergaard yield criterion, and that in plastically deforming near-tip regions plastic strain dominates elastic. Under these assumptions only two types of near-tip plastic solution sector are possible: generalized centered fan, and constant stress (Cartesian components); the appropriate assembly of these provides the complete near-tip stress field. We showed that there are three permissible types of near-tip solution configuration; the applicable one depends on the porosity level, f. One is a generalized Prandtl field which exists for small f, between 0 and $.04468/q_1 \equiv f_1$, and reduces, as $f \to 0$, to the classical Prandtl field of a tensile crack in fully dense Huber-Mises material (Rice, 1967, 1982). Here q_1 is one of the parameters Tvergaard (1981) introduced to improve the Gurson yield condition; it is typically suggested, on the basis of numerical finite element simulations of elastic-plastic response of voided media, that

$q_1 \approx 1.5$ (see Part I). Another near-tip solution type is a plane-stress-like configuration, resembling Hutchinson's (1968) plane stress tensile crack solution for fully dense Huber-Mises material, which exists for $f_1 \leq f \leq 0.18043/q_1 \equiv f_2$. This consists of a generalized centered fan sector beginning at the crack symmetry line, followed by two constant stress plastic sectors with stress jumps in radial and out-of-plane normal components across their mutual border. For the remaining higher porosities $f_2 \leq f \leq 1/q_1$, the stress field is an assembly of two constant stress plastic sectors with stress jumps across their unchanged mutual border; this configuration exists for the entire porosity range from 0 to $1/q_1$.

Among these three distinct types of near-tip solution configuration, the generalized Prandtl field is the only one with fully continuous stress fields. Although stress discontinuities in radial and out-of-plane normal components cannot be ruled out on the basis of the elastic-plastic governing equations, and hence the other near-tip configurations *are* valid solutions to these equations and the boundary conditions, one wonders whether a continuous stress field can also be found for f larger than f_1, which is far below, e.g., the critical value $f \approx 0.15$ suggested by Tvergaard and Needleman (1984), on the basis of comparisons with experiments, to correspond to the onset of substantial void coalescence. Thus the objective of this work is to seek for $f > f_1$ possible completely continuous stress fields by relaxing the assumption that the material experiences plastic response at all angles about the tip, while maintaining the other assumptions reviewed above. Hence possible near-tip solution sector types for $f > f_1$ include the plastic generalized centered fan and constant stress types already analyzed, and now in addition a sector of purely elastic response.

Solutions involving such elastic sectors for stationary crack-tip fields in elastic-plastic materials have been exhibited in other contexts. For example, Gao's (1980) asymptotic mixed-mode plane strain near-tip solutions exhibited these, and Sakata et al.'s (1986) numerical finite element analysis of the same problem class also displayed a near-tip sector of elastic response. In a situation more similar to the present problem, Dong and Pan (1991) analyzed near-tip plane strain tensile crack fields in an elastic-plastic pressure-sensitive model based on a simple yield criterion that is a linear combination of the effective and hydrostatic stresses. For nonhardening materials, their solutions exhibit sectors of elastic response adjacent to the crack flanks, as do our solutions.

We here continue to consider a plane strain Mode I stationary crack in porous elastic-ideally plastic material with spherical microvoids uniformly distributed in the three dimensions so that the material is macroscopically homogeneous, isotropic, and hence so are its overall, or effective, elastic moduli. We assume that the material obeys Tvergaard's (1981, 1982) modification of Gurson's (1977) yield criterion and associated plastic flow rule, and we employ a small-displacement-gradient formulation. Thus for the same reasons stated in Section 7 of Part I, on the basis of full-field numerical finite element solutions referenced there, the present results are expected to be physically meaningful in an annular region surrounding a crack tip, whose inner radius is on the order of two to three times the crack-tip opening displacement and whose outer radius is sufficiently small compared with, e.g., the maximum plastic zone radius. For purely elastic deformations, generalized Hooke's Law is written in terms of the effective (macroscopic) moduli E (Young's modulus) and ν (Poisson's ratio) and hence applies to macroscopic stresses and strains.

Similarly to Part I, let Cartesian axes x_1, x_2 and x_3 be chosen so that x_3 and x_1 are parallel, respectively, to the crack front and the crack surfaces, the latter being assumed traction-free. Throughout the paper, components of tensors with respect to this Cartesian system will be denoted by Latin indices i, j, k, l with range 1, 2, 3; the summation convention for repeated subscripts applies to these indices. Let r, θ be polar coordinates
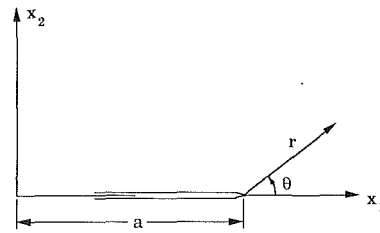

Fig. 1   Cartesian coordinates x_1, x_2, x_3 are fixed in the body; polar coordinates r, θ are centered at the crack tip; a measures crack length
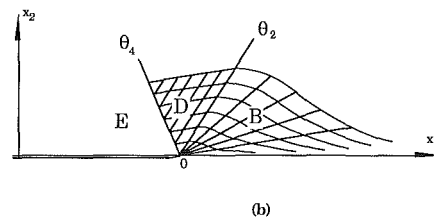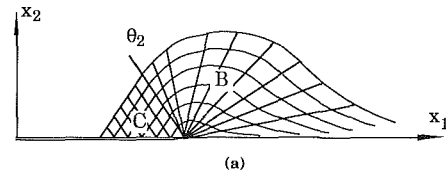

(a)

(b)

Fig. 2   (a) The limiting ($f = f_1$) generalized Prandtl stress field in terms of stress characteristics ($\theta_2 \approx 2.3378$); (b) the continuous asymptotic stress field configuration in terms of stress characteristics for $f_1 < f < 1/q_1$

in the x_1-x_2 plane and centered at the crack tip with $\theta = 0$ coinciding with the positive x_1-axis, as shown in Fig. 1.

As explained in Part I, the three types of fully plastic near-tip sector configuration derived there evolve consistently from one to the next as the porosity level increases. It is thus desired that the new continuous solutions for $f > f_1$ we seek here would reduce, as f approaches f_1 from above, to the limiting generalized Prandtl field that applies at $f = f_1$, as illustrated in Fig. 2(a). On the other hand, the structure of the plane-stress-like distribution, which is obtained by adding a plastic constant stress sector to the configuration of Fig. 2(a) for $f > f_1$, implies that a possible configuration for a *continuous* stress field for $f > f_1$ could be one or both of the following assemblies of those three different sectors: a generalized centered fan plastic sector B, beginning at the symmetry line ($\theta = 0$), followed either by a constant stress plastic sector D and then an elastic sector E adjacent to the crack surface, as shown in Fig. 2(b); or, by an elastic sector first and then a constant stress plastic sector which ends at the crack surface. However, numerical computations show that a solution with this latter configuration cannot exist because full stress continuity, stress symmetry and the traction-free crack surface boundary conditions demand a number of restrictions greater than that of the total undetermined constants; hence all the restrictions cannot be satisfied simultaneously. Thus, we shall investigate the first configuration in this paper. We define θ_2 and θ_4 to be the mutual borders between Sectors B and D, and D and E, respectively, as shown in Fig. 2(b).

2   Asymptotic Governing Equations and Stress Distributions

As noted in the Introduction, we have made here the same assumptions in plastically deforming near-tip sectors as we did

in Part I. Thus, the asymptotic governing equations in such sectors are exactly the same as those previously derived, and so are their stress field solutions; these are reviewed as in the following. Stresses in a purely elastic sector (with no prior plastic straining) are derived here; they must satisfy the equilibrium equations, plane strain and compatibility conditions, and meanwhile must not violate the yield condition.

2.1 Near-Tip Plastic Sectors. We showed in Part I that the asymptotic ($r \to 0$) governing equations in plastically deforming near-tip sectors with singular straining are

$$[\sigma'_{rr} + \sigma'_{\theta\theta}]\left\{3s_{rr} + q_1 q_2 f \sinh\left[\frac{q_2 \sigma_{kk}}{2}\right]\right\} = 0 \qquad (1a)$$

$$3s_{33} + q_1 q_2 f \sinh\left[\frac{q_2 \sigma_{kk}}{2}\right] = 0 \qquad (1b)$$

$$\sigma_{rr} - \sigma_{\theta\theta} + \sigma'_{r\theta} = 0, \quad \sigma'_{\theta\theta} + 2\sigma_{r\theta} = 0 \qquad (1c)$$

$$\sigma'_{11} \sin\theta = \sigma'_{12}\cos\theta, \quad \sigma'_{22}\cos\theta = \sigma'_{12}\sin\theta, \qquad (1d)$$

where (1b) is the plane strain condition; (1c) and (1d) are the equilibrium equations in polar and Cartesian coordinates, respectively; and (1a) is a differential form of the Gurson-Tvergaard yield condition, having employed (1b). Stress components σ_{ij} are normalized by the matrix material's uniaxial yield stress. The notation σ'_{ij} is defined as

$$\sigma'_{ij} \equiv \lim_{r \to 0} \frac{\partial \sigma_{ij}(r, \theta)}{\partial \theta}, \qquad (1e)$$

and $s = \sigma - I\,\text{trace}(\sigma)/3$ is the deviatoric stress tensor with I being the identity tensor.

As detailed in Part I, the only possible solutions to this equation set are plastic sectors in the form of either:

(*i*) *generalized centered fan type*, when the braced term in (1a) vanishes, and (1b) and (1c) are satisfied. When this sector type begins at the symmetry line $\theta = 0$, the stresses are obtained by numerical integration of the rearranged asymptotic governing equations:

$$\sigma_{33} = \sigma_{rr} \qquad (2a)$$

$$\sigma'_{r\theta} = \sigma_{\theta\theta} - \sigma_{rr} \qquad (2b)$$

$$\sigma'_{\theta\theta} = -2\sigma_{r\theta} \qquad (2c)$$

$$\sigma'_{rr} = \sigma_{r\theta} \frac{q_1 q_2^2 f \cosh\left[q_2\left(\sigma_{rr} + \frac{1}{2}\sigma_{\theta\theta}\right)\right] - 2}{q_1 q_2^2 f \cosh\left[q_2\left(\sigma_{rr} + \frac{1}{2}\sigma_{\theta\theta}\right)\right] + 1}, \qquad (2d)$$

with the following boundary values at $\theta = 0$ (explained in Part I):

$$\sigma_{r\theta}(0) = 0 \qquad (3a)$$

$$\sigma_{\theta\theta}(0) = \frac{2}{3}\left[Q + \frac{1}{q_2}\ln\left\{[(1 + q_2^2)(1 + q_1^2 q_2^2 f^2)]^{1/2}\right.\right.$$
$$\left.\left. - 1 + q_2 Q\right\} - \frac{1}{q_2}\ln(q_1 q_2^2 f)\right] \qquad (3b)$$

$$\sigma_{33}(0) = \sigma_{rr}(0) = \sigma_{\theta\theta}(0) - Q \qquad (3c)$$

where

$$Q = \frac{1}{q_2}\left\{2 + q_2^2(1 + q_1^2 f^2) - 2[(1 + q_2^2)(1 + q_1^2 q_2^2 f^2)]^{1/2}\right\}^{1/2}; \qquad (3d)$$

or:

(*ii*) *constant stress plastic type*, when the first bracket in (1a) vanishes, and (1b) and (1d) are satisfied (characterized

by $\sigma_{11} = \text{constant}$, $\sigma_{22} = \text{constant}$, $\sigma_{12} = \sigma_{21} = \text{constant}$, and σ_{33} is also proved to be constant; see Part I). The polar components of stress thus have general (asymptotic) closed-form representations in terms of the variable θ and integration constants c_n (which must satisfy the plane strain condition (1b) and the yield condition):

$$\sigma_{rr} = c_1 + c_2 \cos 2\theta + c_4 \sin 2\theta \qquad (4a)$$

$$\sigma_{\theta\theta} = c_1 - c_2 \cos 2\theta - c_4 \sin 2\theta \qquad (4b)$$

$$\sigma_{r\theta} = -c_2 \sin 2\theta + c_4 \cos 2\theta \qquad (4c)$$

$$\sigma_{33} = c_3. \qquad (4d)$$

2.2 Near-Tip Elastic Sectors. As mentioned in the Introduction, generalized Hooke's Law in terms of effective elastic moduli applies here to macroscopic stresses and strains. This and the plane strain condition together imply

$$\sigma_{33} = \nu(\sigma_{rr} + \sigma_{\theta\theta}) \qquad (5)$$

with which the compatibility equation in terms of stresses without body forces becomes, for arbitrary elastic moduli

$$\left(\frac{\partial^2}{\partial r^2} + \frac{1}{r}\frac{\partial}{\partial r} + \frac{1}{r^2}\frac{\partial^2}{\partial \theta^2}\right)(\sigma_{rr} + \sigma_{\theta\theta}) = 0. \qquad (6)$$

It was proved in Part I that all components of stress at an arbitrary material point must be bounded; thus, a result proved by Drugan (1985) applies:

$$r\frac{\partial \sigma_{ij}}{\partial r} = o\left(\frac{1}{\ln(R/r)}\right) \quad \text{as} \quad r \to 0, \qquad (7)$$

where R is a constant with length dimensions. Taking an r-partial derivative of this, multiplying the resulting equation by r, and then applying (7) gives

$$r^2\frac{\partial^2 \sigma_{ij}}{\partial r^2} = o\left(\frac{1}{\ln(R/r)}\right) \quad \text{as} \quad r \to 0. \qquad (8)$$

Therefore, after multiplying (6) by r^2, applying these asymptotic relations (7) and (8) to the resulting equation, and using notation like that of (1e) (i.e., $\sigma''_{ij} \equiv \lim_{r\to 0}[\partial^2 \sigma_{ij}(r, \theta)/\partial \theta^2]$), the compatibility condition (6) takes the asymptotic ($r \to 0$) form

$$\sigma''_{rr}(\theta) + \sigma''_{\theta\theta}(\theta) = 0. \qquad (9)$$

Hence the asymptotic governing equations in an elastic sector are the equilibrium Eqs. (1c), the plane-strain condition (5) and compatibility (9), which have the following general solution for stresses in terms of the variable θ and integration constants A, B, C, and D:

$$\sigma_{rr}(\theta) = D + 2C\theta + A\cos 2\theta + B\sin 2\theta \qquad (10a)$$

$$\sigma_{\theta\theta}(\theta) = D + 2C\theta - A\cos 2\theta - B\sin 2\theta \qquad (10b)$$

$$\sigma_{r\theta}(\theta) = -C - A\sin 2\theta + B\cos 2\theta \qquad (10c)$$

$$\sigma_{33}(\theta) = 2\nu(D + 2C\theta). \qquad (10d)$$

These elastic sector stress expressions are the same as those obtained by Gao (1980) who simply *assumed* an asymptotic form for the Airy stress function.

3 Asymptotic Sector Assembly Procedure

We now attempt to establish a completely continuous asymptotic stress field for $f > f_1$ by near-tip assembly, in the manner illustrated in Fig. 2(b), of these three different stress sectors: a generalized centered fan, a constant stress plastic sector, and an elastic stress distribution. Hence all parameters to be determined are: A, B, C, D in (10); c_1, c_2, c_3, c_4 in (4); and θ_2 and θ_4 of Fig. 2(b). As shown in Part I, the governing equations require *all* components of stress to be continuous across the mutual border between a constant stress plastic sector and a generalized centered fan plastic sector (i.e., $\theta = \theta_2$), which, together with the assumption of stress continuity across the mu-

tual border between Sectors D and E (i.e., $\theta = \theta_4$) and the traction-free crack-face conditions, will be applied to determine all these unknown parameters. The parameters must be chosen such that $\theta_4 \geq \theta_2$ and the yield condition is not violated in Sector E, for a physically appropriate solution to exist.

Evidently, full stress continuity results in

$$[\![\sigma_{\theta\theta} + \sigma_{rr}]\!] = 0 \quad \text{across} \quad \theta = \theta_2, \theta_4, \tag{11}$$

where

$$[\![\sigma(\theta)]\!] \equiv \sigma(\theta^+) - \sigma(\theta^-); \tag{12}$$

(11) leads, via (10a,b) and (4a,b), to

$$2c_1 = 2(D + 2C\theta_4) \tag{13a}$$

$$2c_1 = \sigma_{\theta\theta}(\theta_2^-) + \sigma_{rr}(\theta_2^-). \tag{13b}$$

Furthermore, continuity of σ_{33} across $\theta = \theta_2, \theta_4$ together with (10d), (4d), and (2a) gives

$$c_3 = 2\nu(D + 2C\theta_4) = \sigma_{rr}(\theta_2^-), \tag{14}$$

which, via (13), implies

$$\sigma_{\theta\theta}(\theta_2^-) = \frac{1-\nu}{\nu} \sigma_{rr}(\theta_2^-). \tag{15}$$

Application of this condition to the numerical integration of (2) in the generalized centered fan sector determines the value of θ_2, showing where that sector ends. The other unknown parameters in Sector D of Fig. 2(b) are then immediately determined by enforcing full stress continuity across θ_2, which implies that both the plane strain and yield conditions are automatically satisfied and results in

$$c_1 = \frac{1}{2} [\sigma_{\theta\theta}(\theta_2^-) + \sigma_{rr}(\theta_2^-)] \tag{16a}$$

$$c_2 = -\sigma_{r\theta}(\theta_2^-)\sin 2\theta_2 + \frac{1}{2}[\sigma_{rr}(\theta_2^-) - \sigma_{\theta\theta}(\theta_2^-)]\cos 2\theta_2 \tag{16b}$$

$$c_3 = \sigma_{rr}(\theta_2^-) \tag{16c}$$

$$c_4 = \sigma_{r\theta}(\theta_2^-)\cos 2\theta_2 + \frac{1}{2}[\sigma_{rr}(\theta_2^-) - \sigma_{\theta\theta}(\theta_2^-)]\sin 2\theta_2. \tag{16d}$$

To determine the remaining unknown parameters, we first apply the traction-free boundary conditions at $\theta = \pi$ using (10b,c):

$$B = C; \quad A = D + 2\pi C. \tag{17a,b}$$

Also, continuity of $(\sigma_{rr}(\theta) - \sigma_{\theta\theta}(\theta))$ and $\sigma_{12}(\theta)$ across θ_4 altogether with (17), (10a,b,c) and (4a,b,c) results in

$$[c_2 - (D + 2\pi C)]\cos 2\theta_4 + (c_4 - C)\sin 2\theta_4 = 0 \tag{18a}$$

$$C(1 - \cos 2\theta_4) = c_4. \tag{18b}$$

Obviously, for $\theta_4 \neq 0$ or π, the above can be solved for D and C in terms of c_2, c_4 and θ_4; these expressions are used in (13a) to obtain an algebraic equation for θ_4 alone. The resulting equations are

$$c_1 - c_2 + c_4 \frac{\sin 2\theta_4 + 2(\pi - \theta_4)}{1 - \cos 2\theta_4} = 0 \tag{19}$$

$$D = c_2 - \frac{\sin 2\theta_4 + 2\pi}{1 - \cos 2\theta_4} c_4 \tag{20a}$$

$$C = \frac{1}{1 - \cos 2\theta_4} c_4. \tag{20b}$$

By solving (19) numerically (having substituted (16)), satisfying $0 \leq \theta_2 \leq \theta_4 \leq \pi$, the parameters A, B, C, D will be determined by using (20) and then (17). These results are acceptable if and only if the stresses in (10) with the coefficients given by (20) and (17) do not violate yield for all $\theta_4 \leq \theta \leq \pi$.

As far as the special case $\theta_4 = \pi$ is concerned, one observes that in the limit $\theta_4 \to \pi$, l'Hopital's rule shows that in (19) the term $[\sin 2\theta_4 + 2(\pi\theta_4)]/[1 - \cos 2\theta_4]$ has a limit of zero, which

together with the boundedness of all the c_n's given by (16) implies

$$\lim_{\theta_4 \to \pi} c_1 = \lim_{\theta_4 \to \pi} c_2. \tag{21}$$

On the other hand, (18a) and (13a) show, via (21) and the boundedness of c_4, that $C \sin 2\theta_4 \to 0$, or $C = o(1/\sin \theta_4)$ as $\theta_4 \to \pi$. Application of this asymptotic equation to (18b) further implies that $c_4 = o(\sin \theta_4)$; that is

$$\lim_{\theta_4 \to \pi} c_4 = 0. \tag{22}$$

Evidently, (21) and (22) show that $\theta_4 = \pi$ would result in a physically appropriate solution if and only if $c_1 = c_2$ and $c_4 = 0$, which are indeed the two traction-free conditions on the crack surface when the elastic sector vanishes, and thus the constant stress Sector D ends at the crack surface. In this situation, the features of stresses in Sector D here and those in Sector C in the limiting generalized Prandtl field of Fig. 2(a) are the same. Numerical calculations show that this situation can occur, with the complete solution reducing precisely to the limiting Prandtl field, if and only if the porosity f decreases to f_1. This indicates a smooth evolution from the continuous generalized Prandtl field to the current continuous solution.

Now consider the other special case, namely $\theta_4 = 0$. As a limiting case of the solution having the configuration of Fig. 2(b), this could be true only if $\theta_2 = 0$ holds as well, which requires $\nu = \sigma_{rr}(0)/[\sigma_{\theta\theta}(0) + \sigma_{rr}(0)]$ as detailed later. Consequently, (16d) gives $c_4 = 0$ and thus (18b) demands C be finite, while (18a) and (13a) together imply $D = c_1$ and $C = (c_1 - c_2)/2\pi$. With these and (17) and the particular value of ν as well, full stress continuity across the internal borders is satisfied and so are the traction-free crack surface and stress symmetry conditions. However, the numerical computations to be described show that this purely elastic stress field as a limiting case of the solution we seek here cannot occur.

4 Existence of the Solution and Solvability Conditions

In order to obtain a complete stress field with the assumed configuration shown in Fig. 2(b) it is necessary for the key Eqs. (15) and (19), which determine the sector boundary locations θ_2 and θ_4, respectively, to have solutions satisfying the basic requirement

$$0 \leq \theta_2 \leq \theta_4 \leq \pi. \tag{23}$$

We first prove that for each fixed value of f in the range

$$f_1 \leq f < 1/q_1, \tag{24}$$

(15) has a unique solution for θ_2 for a certain *range* of Poisson's ratios. Recalling the plane strain condition in the generalized centered fan sector (see Part I), we have

$$\sigma_{\theta\theta} - \sigma_{rr} = q_1 q_2 f \sinh\left[q_2\left(\sigma_{rr} + \frac{1}{2}\sigma_{\theta\theta}\right)\right]. \tag{25}$$

With reference to the numerical calculations of Part I, we found that for every fixed f satisfying (24), there is a unique $0 < \bar{\theta}(f) < \pi$ in a generalized centered fan sector bordering $\theta = 0$ such that $\sigma_{kk}(\bar{\theta}) = 0$ and $\sigma_{\theta\theta}(\bar{\theta}) = 0 = \sigma_{rr}(\bar{\theta})$; and for all $0 \leq \theta < \bar{\theta}(f)$, $\sigma_{kk}(\theta) > 0$, $\sigma_{rr}(\theta) > 0$ and $\sigma_{\theta\theta}(\theta) > 0$, which together with (25) indicates $\sigma_{\theta\theta}(\theta) > \sigma_{rr}(\theta)$. Also, the continuous function $\sigma_{\theta\theta}(\theta)/\sigma_{rr}(\theta)$ decreases monotonically as θ increases. Thus by using these results and rewriting (15) as

$$\frac{1}{\nu} = 1 + \frac{\sigma_{\theta\theta}(\theta_2^-)}{\sigma_{rr}(\theta_2^-)}, \tag{26}$$

one can easily find that $1 + [\sigma_{\theta\theta}(\theta_2^-)/\sigma_{rr}(\theta_2^-)] > 2$, and hence for each f in the range (24) and each $\sigma_{rr}(0)/[\sigma_{\theta\theta}(0) + \sigma_{rr}(0)] \leq \nu < (1/2)$, there is a unique $\theta_2 \in (0, \bar{\theta}(f))$ such that (26), or (15), holds; and the larger the ν, the larger the value of θ_2. It is noticed that for $\theta_2 = 0$ with $\nu = \sigma_{rr}(0)/[\sigma_{\theta\theta}(0) + \sigma_{rr}(0)]$, the generalized

centered fan sector vanishes. It is also noticed that ν must be less than 1/2, which means that the porous material considered here must also be elastically compressible. In fact, as mentioned in the Introduction, for porous materials the ν used here is indeed the macroscopic (effective) Poisson's ratio and hence it is smaller than that of the matrix material, even if the matrix material is elastically incompressible, because material with nonzero porosity is no longer macroscopically elastically incompressible.

To investigate conditions under which (19) will have solutions $\theta_4 \epsilon (0, \pi)$, we first rewrite it, for $c_4 \neq 0$, as

$$\frac{c_1 - c_2}{c_4} + \frac{\sin 2\theta_4 + 2(\pi - \theta_4)}{(1 - \cos 2\theta_4)} = 0, \qquad (27)$$

and we define

$$\alpha = \frac{c_1 - c_2}{c_4}, \qquad (28a)$$

$$G(x, \alpha) = \alpha + \frac{\sin 2x + 2(\pi - x)}{(1 - \cos 2x)}. \qquad (28b)$$

Thus the root of Eq. (27) is the same as the zero point of the function $G(x, \alpha)$; the latter can be more easily studied by analyzing the features of $G(x, \alpha)$. Evidently, via (28b), we have for each fixed α

$$G(0, \alpha) = +\infty, \quad G(\pi, \alpha) = \alpha. \qquad (29)$$

Also the function $G(x, \alpha)$ decreases monotonically on the interval $[0, \pi]$ for each fixed α since for every $x \epsilon (0, \pi)$ its first-order derivative with respect to x is always negative:

$$\frac{\partial G}{\partial x}(x, \alpha) = -\frac{2}{\sin^3 x}[\sin x + \cos x(\pi - x)] < 0. \qquad (30)$$

Hence, (27) will have a unique solution on the interval $(0, \pi)$ if and only if $\alpha < 0$, which via (28a) requires $(c_1 - c_2)/c_4 < 0$ (according to (4), this means that σ_{22} and σ_{12} in the constant stress plastic Sector D must have opposite signs), and it will have a root $x = \pi$ and $\alpha = 0$. This latter case, as mentioned earlier, cannot result in an acceptable stress field unless both the conditions $c_1 = c_2$ for $c_4 = 0$, representing the traction-free boundary conditions, can be satisfied.

As regards the special situation $c_4 = 0$, (18b) demands either $C = 0$, or $\theta_4 = 0$ or π. With $C = 0$ and $c_4 = 0$, (17a) gives $B = 0$; (18a) and (17b) require $A = D = c_2$, while 13(a) and (17b) demand $A = D = c_1$. Thus if $c_1 \neq c_2$, no such solution can exist; otherwise (10) gives, after substituting all these results for those parameters, exactly the same stress distribution in the elastic Sector E as that in the constant stress Sector D given by (4) with $c_4 = 0$ and $c_1 = c_2$. In this case, θ_4 is arbitrary, and indeed Sectors E and D join to become one constant stress plastic sector; the features of the entire stress field are hence similar to those of the limiting Prandtl field of Fig. 2(a) (see Part I). Similarly, as in Section 3, $\theta_4 = \pi$ with $c_4 = 0$ may lead to a solution if and only if $c_1 = c_2$. As mentioned previously, this will take place only when f approaches f_1. However, with $\theta_4 = 0$, one has to require $\theta_2 = 0$, otherwise no solution will exist.

Thus we have shown that there is a unique θ_2 for each f in the range (24) and some $\sigma_{rr}(0)/[\sigma_{\theta\theta}(0) + \sigma_{rr}(0)] < \nu < 1/2$; and with $(c_1 - c_2)/c_4 < 0$ there is a unique $\theta_4 \epsilon (0, \pi)$. As long as (23) is satisfied and yield is not violated in the elastic Sector E, an acceptable solution for such an f and ν is thus found.

5 Results

Since the stresses in the generalized centered fan sector must be determined by numerical integration, all the unknown parameters satisfying (15), (16), (17), (19), (20), and (23) are thus numerically determined. The results show that a stress field with the configuration illustrated in Fig. 2(b) does exist for all f in the range (24) and for certain ranges of Poisson's ratio

which depend on the value of f. The results also indicate that the locations of both internal boundaries θ_2 and θ_4 and the angular extent of each of the sectors are strongly influenced by not only the void volume fraction f but also Poisson's ratio ν: both θ_2 and θ_4 decrease as f increases (see Table 1); but for each fixed f, they increase as Poisson's ratio does on its corresponding range, as do the angular spans of the constant stress plastic Sector D and the generalized centered fan Sector B. The angular extent of the elastic Sector E decreases as ν increases. These trends will be seen in Figs. 3 and 4.

As regards the solution existence range, the results clearly indicate that for each f in the range (24), there is a smallest value of ν, which is larger than $\sigma_{rr}(0)/[\sigma_{\theta\theta}(0) + \sigma_{rr}(0)]$ and is here called ν_{min}, at which $\theta_4 = \theta_2$, meaning the constant stress plastic Sector D vanishes, and below which $\theta_4 < \theta_2$ so that the solution does not hold. In this situation, both θ_4 and θ_2 attain their smallest values over the interval (ν_{min}, ν_{max}), as defined later. Similarly, there is a ν_{max} such that if $\nu > \nu_{max}$, the yield condition is violated in the elastic sector. Values of both ν_{min} and ν_{max} are dependent on the void volume fraction f, which indicates in one way the inner link between the macroscopic elastic moduli and the porosity level. Therefore, the solution exists only on the interval (ν_{min}, ν_{max}), and the extent of this interval varies with f: it is nearly 0 in the limits $f \to f_1$ and $f \to 1/q_1$. It is also observed that both the values of ν_{min} and ν_{max} decrease as f increases. This ν_{max} is smaller than 1/2, the value of Poisson's ratio for elastically incompressible materials; this shows that in the present $f > 0$ analysis the material must be macroscopically elastically compressible for a solution to exist.

Since the solution can exist only for $\nu \leq \nu_{max}(f)$, one wonders what this $\nu_{max}(f)$ means. Does it correspond to the actual
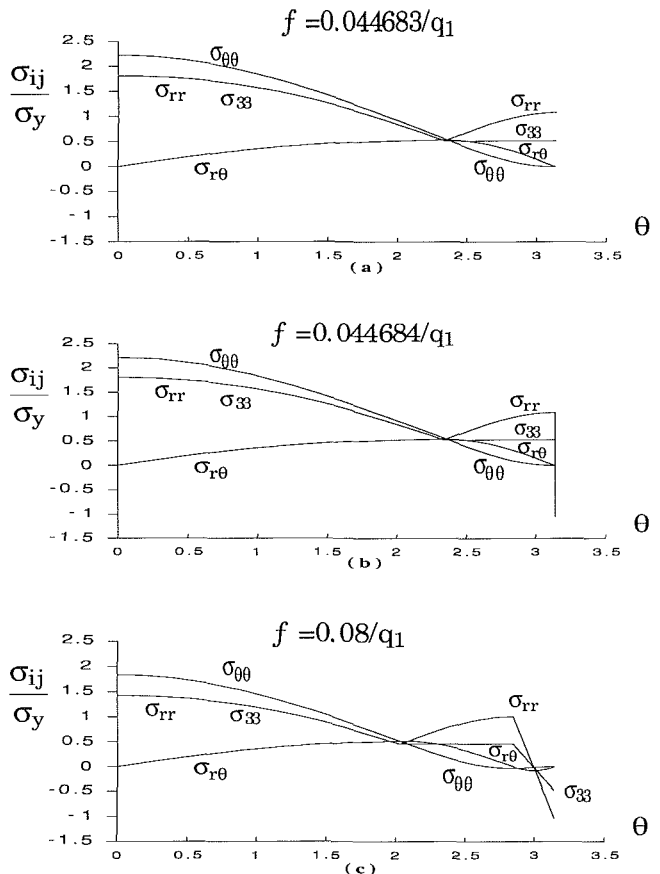

Fig. 3 Polar components of stress as functions of angle θ with the solution configuration of Fig. 2(b): (a) for $f = f_1$ (or, $f \to f_1^+$), with $\nu \approx .481611$, $\theta_2 \approx 2.3378$, $\theta_4 \approx \pi$; (b) for $f \approx .044684/q_1$, with $\nu \approx .481610$, $\theta_2 \approx 2.33779$, $\theta_4 \approx 3.14157$; (c) for $f \approx .08/q_1$, with $\nu \approx .468081$, $\theta_2 \approx 2.02623$, $\theta_4 \approx 2.84110$

effective Poisson's ratio for this porous material? The approximate effective elastic moduli in porous material have been investigated by several researchers including, for example, Zhao et al. (1989). By employing their work, we determine the effective Poisson's ratio, ν_e (see the Appendix and Table 1), for the porous material considered in this study. Specifically, when the matrix material is assumed to be elastically incompressible, as in our solutions, ν_e values for small f are very close to our ν_{max}. For instance, for $f = f_1$, the relative difference $(\nu_e - \nu_{max})/\nu_{max} \approx .006$; and for $f \approx .25/q_1$, $(\nu_e - \nu_{max})/\nu_{max} \approx .061$. These comparisons show that $\nu_{max}(f)$ appears to be the actual effective Poisson's ratio for a given f. Both ν_e and ν_{max} for selected f values are shown in Table 1.

An interesting related phenomenon is that as $f \to f_1$, θ_2 and θ_4 corresponding to $\nu_{max}(f) = .481611$ approach 2.3378 and π, respectively, and the elastic sector vanishes in this limit. Also conditions (21) and (22) are satisfied. This shows that the solution family corresponding to the set of $\nu_{max}(f)$ reduces to the limiting generalized Prandtl field of Fig. 2(a), derived in
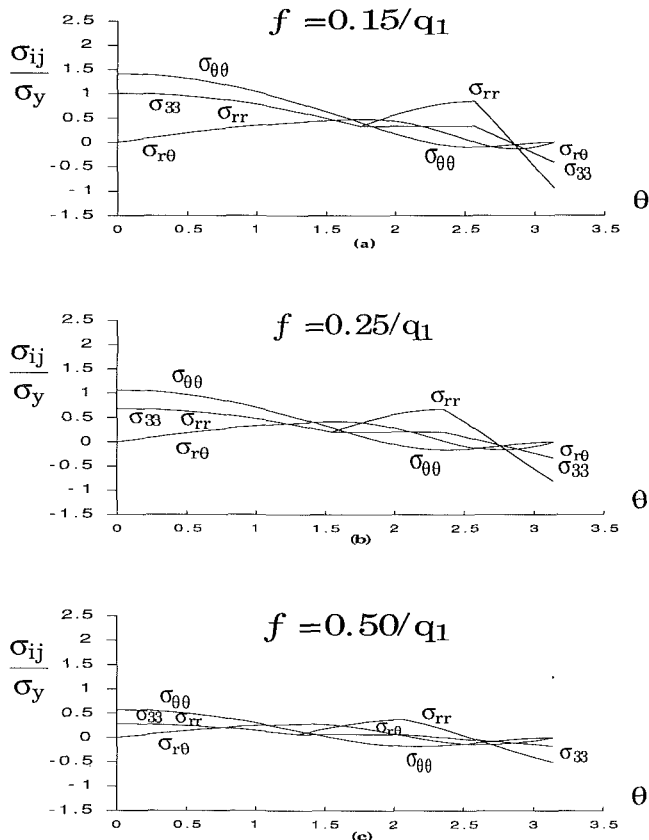
Part I, as $f \to f_1$. Thus this solution family will be taken as the new continuous solutions for those porosities in the range (24), since it evolves consistently from the generalized Prandtl field. Stress distributions for selected values of f corresponding to this solution family having $\nu = \nu_{max}$ are displayed in Figs. 3 and 4.

One observes, see e.g., Fig. 3(b), that for f very close to f_1^+, the angular extent of the elastic sector is almost zero: for $f \approx f_1 + 1.0 \times 10^{-6}/q_1$, $\theta_4 \approx \pi - 2.0 \times 10^{-5}$ rad., and stress components σ_{rr} and σ_{33} seem to "jump" from positive to negative values within a small transition zone of angular width less than 2.0×10^{-5} radian. As f increases, θ_4 corresponding to $\nu_{max}(f)$ decreases (see Table 1) so that the angular span of the elastic sector increases, and the apparent "stress jump" is smoothed out.

The solution configuration shown in Fig. 2(b) is maintained for all f in the range (24). In addition, as predicted by the yield criterion, the magnitudes of the stress components and the hydrostatic stress decrease as the porosity level increases. That this decrease in hydrostatic stress level with increasing porosity is substantial is illustrated in Fig. 5, which shows hydrostatic stress directly ahead of the tip as a function of f. The superscripts I and II correspond to the predictions from the fully plastic solutions of Part I and those of the present solutions, respectively. The close agreement between these two predictions is remarkable, especially over the practically important range of, say, $0 \le f \le 0.15$.

Comparing Fig. 5 in Part I with Fig. 3 here, one observes that the border between the generalized centered fan sector and the constant stress plastic sector shifts backward substantially, and what were stress jumps in the fully plastic solutions are now rapid but continuous variations in the elastic stress sector. Thus the extent of the generalized centered fan sector

Fig. 4 Polar components of stress as functions of angle θ with the solution configuration of Fig. 2(b) (continued): (a) for $f \approx .15/q_1$, with $\nu \approx .443256$, $\theta_2 \approx 1.73909$, $\theta_4 \approx 2.56225$; (b) for $f \approx .25/q_1$, with $\nu \approx .409936$, $\theta_2 \approx 1.53475$, $\theta_4 \approx 2.35114$; (c) for $f \approx .50/q_1$ with $\nu \approx .332823$, $\theta_2 \approx 1.29846$, $\theta_4 \approx 2.05549$
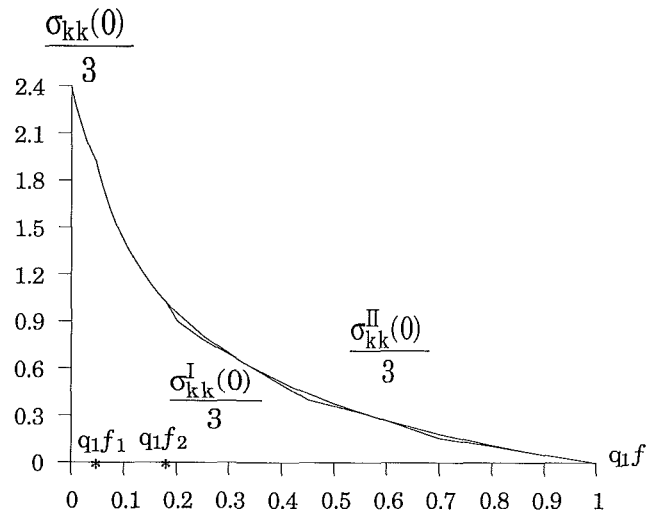

Fig. 5 Hydrostatic stress level (normalized by the matrix material's uniaxial yield stress) directly ahead of the crack tip versus void volume fraction, as predicted by the fully plastic solutions of Part I (superscript I) and the present elastic-plastic solutions (superscript II).

Table 1 Parameter values for fully continuous stress field solutions having the configuration of Fig. 2(b) ($f \ge f_1$)

$q_1 f$	θ_2(rad)	θ_4(rad)	c_1	c_2	c_3	c_4	A	B=C	D	ν_{max}	ν_e
.044683	2.33780	3.14159	.5422	.5422	.52222	.00000				.48161	.48449
.044684	2.33779	3.14156	.54216	.54216	.52222	-.00001	-.63863	-13442	84458	.48161	.48449
.080000	2.02623	2.84110	.48623	.42701	.45519	-.29207	-.51550	-1.6668	9.9574	.46808	.47379
.150000	1.73909	2.56225	.37092	.19598	.32883	-.43262	-.46529	-.72169	4.0692	.44326	.45574
.250000	1.53475	2.35114	.25710	.01618	.21079	-.41887	-.39847	-.41468	2.2070	.40994	.43541
.500000	1.29846	2.05549	.10788	-.11400	.07181	-.25779	-.24974	-.16463	.78469	.33282	.40146

is enlarged, the magnitude of the stress in the constant stress plastic sector is reduced and hence the stresses become negative near the crack surfaces.

Acknowledgments

References

Dong, P., and Pan, J., 1991, "Elastic-Plastic Analysis of Cracks in Pressure-Sensitive Materials," *International Journal of Solids and Structures*, Vol. 28, pp. 1113–1127.

Drugan, W. J., 1985, "On the Asymptotic Continuum Analysis of Quasi-Static Elastic-Plastic Crack Growth and Related Problems," ASME JOURNAL OF APPLIED MECHANICS, Vol. 52, pp. 601–605.

Drugan, W. J., and Miao, Y., 1992, "Influence of Porosity on Plane Strain Tensile Crack Tip Stress Fields in Elastic-Plastic Materials: Part I," ASME JOURNAL OF APPLIED MECHANICS, Vol. 59, pp. 559–567.

Gao, Y. C., 1980, "Elastic-Plastic Field of a Crack Before Growing in Perfectly Plastic Medium," *Acta Solid Mechanica Sinica*, Vol. 1, pp. 69–75.

Gurson, A. L., 1977, "Continuum Theory of Ductile Rupture by Void Nucleation and Growth: Part I—Yield Criteria and Flow Rules for Porous Ductile Media," ASME *Journal of Engineering Materials and Technology*, Vol. 99, pp. 2–15.

Hutchinson, J. W., 1968, "Plastic Stress and Strain Fields at a Crack Tip," *Journal of the Mechanics and Physics of Solids*, Vol. 16, pp. 337–347.

Rice, J. R., 1967, "Mechanics of Crack Tip Deformation and Extension by Fatigue," *Fatigue Crack Propagation*, ASTM-STP 415, American Society for Testing and Materials, Philadelphia, pp. 247–311.

Rice, J. R., 1982, "Elastic-Plastic Crack Growth," *Mechanics of Solids: The R. Hill 60th Anniversary Volume*, H. G. Hopkins and M. J. Sewell, eds., Pergamon Press, Oxford, pp. 539–562.

Sakata, M., Abe, H., and Tanaka, S., 1986, "Numerical Analysis of Blunting of a Crack Tip in a Ductile Material Under Small-Scale Yielding and Mixed Mode Loading," *Computational Mechanics*, Vol. 1, pp. 11–19.

Tvergaard, V., 1981, "Influence of Voids on Shear Band Instabilities Under Plane Strain Conditions," *International Journal of Fracture*, Vol. 17, pp. 389–407.

Tvergaard, V., 1982, "On Localization in Ductile Materials Containing Spherical Voids," *International Journal of Fracture*, Vol. 18, pp. 237–252.

Tvergaard, V., and Needleman, A., 1984, "Analysis of the Cup-Cone Fracture in a Round Tensile Bar," *Acta Metallurgica*, Vol. 32, pp. 157–169.

Zhao, Y. H., Tandon, G. P., and Weng, G. J., 1989, "Elastic Moduli for a Class of Porous Materials," *Acta Mechanica*, Vol. 76, pp. 105–130.

APPENDIX

The Effective Poisson's Ratio

For a material which is an aggregate of an isotropic elastic matrix and three-dimensional randomly distributed voids, the effective bulk and shear moduli are given approximately, as suggested in Zhao et al. (1989), by

$$\frac{\kappa}{\kappa_0} = \frac{1}{1+fp}, \qquad \frac{\mu}{\mu_0} = \frac{1}{1+fq}, \tag{A1}$$

where p and q are functions of Poisson's ratio, and quantities with or without the subscript "0" denote, respectively, those of matrix material and the corresponding effective one. With reference to Zhao et al. these functions simplify, for spherical voids, to

$$p = \frac{3}{2}\frac{1-\nu_0}{1-2\nu_0}, \qquad q = 14f\frac{1-\nu_0}{7-5\nu_0}. \tag{A2}$$

By using the definition of the bulk modulus and the relation among the elastic moduli, and via (A2), (A1) become

$$\frac{1-2\nu_0}{1-2\nu}\frac{E}{E_0} = \frac{\kappa}{\kappa_0} = \frac{2(1-2\nu_0)}{2(1-2\nu_0)+3f(1-\nu_0)}, \tag{A3a}$$

$$\frac{1+\nu_0}{1+\nu}\frac{E}{E_0} = \frac{\mu}{\mu_0} = \frac{7-5\nu_0}{7-5\nu_0+14f(1-\nu_0)}. \tag{A3b}$$

Elimination of E/E_0 from the above equations and rearrangement of the resulting equation gives the effective Poisson's ratio as a function of that of the matrix material and the void volume fraction:

$$\nu_e = \frac{6(7-5\nu_0)\nu_0 + f(1-\nu_0)(7+43\nu_0)}{6(7-5\nu_0)+f(1-\nu_0)(77+41\nu_0)}. \tag{A4}$$

For an elastically incompressible matrix material ($\nu_0 = 1/2$), the effective Poisson's ratio, via (A4), becomes

$$\nu_e = \frac{18+19f}{36+65f}. \tag{A5}$$